Article

Multigram Scale Synthesis and Characterization of Monodisperse Tetragonal Zirconia Nanocrystals

Jin Joo, Taekyung Yu, Young Woon Kim, Hyun Min Park, Fanxin Wu, Jin Z. Zhang, and Taeghwan Hyeon

J. Am. Chem. Soc., **2003**, 125 (21), 6553-6557• DOI: 10.1021/ja034258b • Publication Date (Web): 01 May 2003

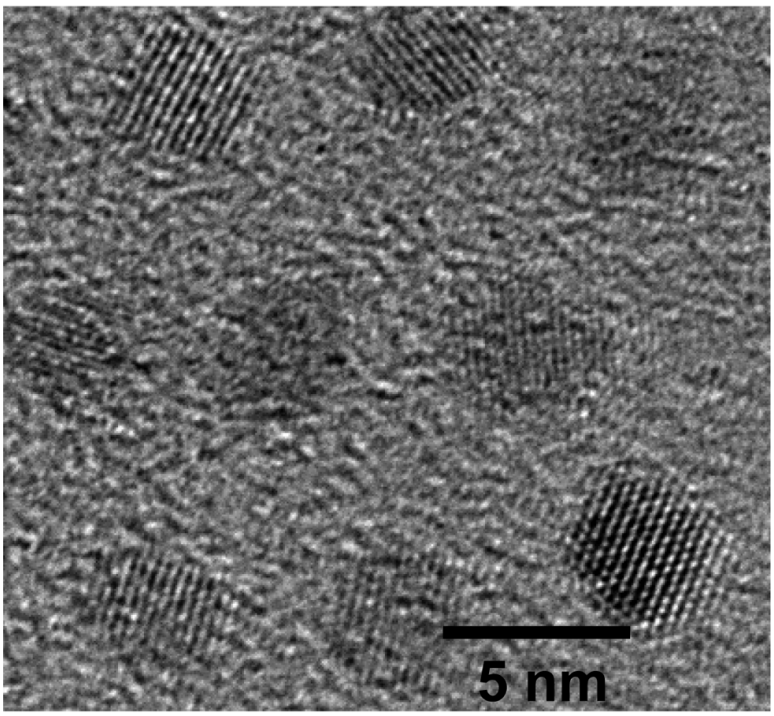

More About This Article

Additional resources and features associated with this article are available within the HTML version:

- Supporting Information
- Links to the 21 articles that cite this article, as of the time of this article download
- Access to high resolution figures
- Links to articles and content related to this article
- Copyright permission to reproduce figures and/or text from this article

J|A|C|S
ARTICLES
Published on Web 05/01/2003

Multigram Scale Synthesis and Characterization of Monodisperse Tetragonal Zirconia Nanocrystals

Jin Joo,[†] Taekyung Yu,[†] Young Woon Kim,[‡] Hyun Min Park,[§] Fanxin Wu,[||] Jin Z. Zhang,[||] and Taeghwan Hyeon*,[†]

Contribution from the National Creative Research Initiative Center for Oxide Nanocrystalline Materials and School of Chemical Engineering, Seoul National University, Seoul 151-744, Korea, School of Materials Science and Engineering, Seoul National University, Seoul 151-744, Korea, New Material Evaluation Center, Korea Research Institute of Standards and Science, Taeduk Science Town, P.O. Box 102, Taejon 305-600, Korea, and Department of Chemistry, University of California, Santa Cruz, California 95064

Received January 21, 2003; E-mail: thyeon@plaza.snu.ac.kr

Abstract: A new and simple method has been developed to synthesize large quantities of highly monodisperse tetragonal zirconia nanocrystals. In this synthesis, a nonhydrolytic sol−gel reaction between zirconium(IV) isopropoxide and zirconium(IV) chloride at 340 °C generated 4 nm sized zirconia nanoparticles. A high-resolution transmission electron microscopic (HRTEM) image showed that the particles have a uniform particle size distribution and that they are highly crystalline. These monodisperse nanoparticles were synthesized without any size selection process. X-ray diffraction studies combined with Rietveld refinement revealed that the ZrO_2 nanocrystals are the high-temperature tetragonal phase, and very close to a cubic phase. When zirconium(IV) bromide is used as a precursor instead of zirconium chloride, zirconia nanoparticles with an average size of 2.9 nm were obtained. The UV−visible absorption spectrum of 4 nm sized zirconia nanoparticles exhibited a strong absorption starting at around 270 nm. A fluorescence spectrum with excitation at 300 nm showed a broad fluorescence band centered around 370 nm. FTIR spectra showed indication of TOPO binding on the ZrO_2 nanoparticle surface. These optical studies also suggest that the nanoparticles are of high quality in terms of narrow particle size distribution and relatively low density of surface trap states.

Nanocrystalline particles have attracted broad attention from researchers in various areas for both their fundamental size-dependent properties and their many important technological applications.[1] These nanocrystalline materials exhibit size-dependent characteristics, and often novel electronic, magnetic, optical, chemical, and mechanical properties that cannot be achieved using their bulk counterparts.[2] Various kinds of nanocrystals have been used for biological labeling and detection,[3] information storage media,[4] lasers,[5] photochemical reactions,[6] and catalysis.[7] Recently, intensive research effort has been focused on the synthesis of well-defined uniform nanocrystals to identify the size-dependent properties.[8−11] As compared to the nanocrystals of II-VI semiconductors and noble metals, relatively little work has been conducted on the synthesis of monodisperse nanocrystals of transition metal oxides despite their many important technological applications.[12]

Zirconia is a very important ceramic material and has found applications in a number of technologies, including fuel cell

[†] National Creative Research Initiative Center for Oxide Nanocrystalline Materials and School of Chemical Engineering, Seoul National University.
[‡] School of Materials Science and Engineering, Seoul National University.
[§] Korea Research Institute of Standards and Science.
[||] University of California.

(1) (a) Weller, H. *Angew. Chem., Int. Ed. Engl.* **1993**, *32*, 41. (b) Schmid, G. *Clusters and Colloids*; VCH Press: New York, 1994. (c) Klabunde, K. J. *Nanoscale Materials in Chemistry*; Wiley-Interscience: New York, 2001. (d) Fendler, J. H. *Nanoparticles and Nanostructured Films*; Wiely-VCH: Weinheim, 1998.
(2) (a) Alivisatos, A. P. *Science* **1996**, *271*, 933. (b) Hyeon, T. *Chem. Commun.* **2003**, 927. (c) Brus, L. E. *J. Chem. Phys.* **1986**, *90*, 2555. (d) Majetich, S. A.; Jin, Y. *Science* **1999**, *284*, 470. (e) Murray, C. B.; Kagan, C. R.; Bawendi, M. G. *Science* **1995**, *270*, 1335.
(3) (a) Bruchez, M.; Moronne, M.; Gin, P.; Weiss, S.; Alivisatos, A. P. *Science* **1998**, *281*, 2013. (b) Taton, T. A.; Mirkin, C. A.; Letsinger, R. L. *Science* **2000**, *289*, 1757. (c) Park, S.-J.; Taton, T. A.; Mirkin, C. A. *Science* **2002**, *295*, 1503. (d) Chan, W. C. W.; Nie, S. M. *Science* **1998**, *281*, 2016.
(4) (a) Black, C. T.; Murray, C. B.; Sandstrom, R. L.; Sun, S. *Science* **2000**, *290*, 1131. (b) Sun, S.; Murray, C. B.; Weller, D.; Folks, L.; Moser, A. *Science* **2000**, *287*, 1989.
(5) (a) Klimov, V. I.; Mikhailovsky, A. A.; Xu, S.; Malko, A.; Hollingsworth, J. A.; Leatherdale, C. A.; Eisler, H.-J.; Bawendi, M. G. *Science* **2000**, *290*, 314. (b) Eisler, H.-J.; Sundar, V. C.; Bawendi, M. G.; Walsh, M.; Smith, H.; Klimov, V. *Appl. Phys. Lett.* **2002**, *80*, 4614.
(6) Hagfeldt, A.; Grätzel, M. *Chem. Rev.* **1995**, *95*, 49.
(7) (a) Kim, S.-W.; Kim, M.; Lee, W. Y.; Hyeon, T. *J. Am. Chem. Soc.* **2002**, *124*, 7642. (b) Kim, S.-W.; Son, S. U.; Lee, S. S.; Hyeon, T.; Chung, Y. K. *Chem. Commun.* **2001**, 2212.
(8) Hyeon, T.; Lee, S. S.; Park, J.; Chung, Y.; Na, H. B. *J. Am. Chem. Soc.* **2001**, *123*, 12798.
(9) Hyeon, T.; Chung, Y.; Park, J.; Lee, S. S.; Kim, Y.-W.; Park, B. H. *J. Phys. Chem. B* **2002**, *106*, 6831.
(10) Murray, C. B.; Norris, D. J.; Bawendi, M. G. *J. Am. Chem. Soc.* **1993**, *115*, 8706.
(11) Chen, C.-C.; Herhold, A. B.; Johnson, C. S.; Alivisatos, A. P. *Science* **1997**, *276*, 398.
(12) (a) Rao, C. N. R.; Raveau, B. *Transition Metal Oxides*, 2nd ed.; Wiley-VCH: New York, 1998. (b) Trentler, T. J.; Denler, T. E.; Bertone, J. F.; Agrwal, A.; Colvin, V. L. *J. Am. Chem. Soc.* **1999**, *121*, 1613. (c) Liu, C.; Zou, B.; Rondinone, A. J.; Zhang, Z. J. *J. Am. Chem. Soc.* **2001**, *123*, 4344. (d) O'Brien, S.; Brus, L.; Murray, C. B. *J. Am. Chem. Soc.* **2001**, *123*, 12086.

electrolytes,[13] high-performance transformation-toughened structural engineering ceramic,[14] catalysts,[15] buffer layers for superconductor growth,[16] oxygen sensor,[17] damage resistant optical coatings,[18] and gate dielectric.[19] Zirconia can adopt three different crystalline structures, that is, cubic, tetragonal, and monoclinic polymorphs. The monoclinic phase, stable at room temperature, is transformed to tetragonal at 1170 °C, and then to cubic at 2370 °C. These two high-temperature phases are unstable in bulk forms at ambient temperature, which is unfortunate because they are more valuable for the technological applications mentioned above than the room-temperature monoclinic phase. Consequently, many divalent and trivalent cationic species such as Mg^{2+}, Ca^{2+}, and Y^{3+} have been incorporated into zirconia to prepare cubic and tetragonal zirconia that is stable at room temperature.[20]

Several different methods have been investigated as routes for the synthesis of zirconia nanoparticles, which include the sol−gel process,[21] spray pyrolysis,[22] mechanochemical processing,[23] salt-assisted aerosol decompositions,[24] carbon nanotube templated method,[25] and emulsion precipitation.[26] However, most of these nanoparticles are poorly crystalline or exhibit broad particle size distributions, and the successful synthesis of uniform-sized undoped zirconia nanocrystals has rarely been reported. In addition, a large-scale synthetic procedure should be developed for the extensive applications of zirconia nanocrystals. Recently, our research group developed a new synthetic procedure for producing highly crystalline and monodisperse ferrite nanocrystals without a size selection process. As part of our continuing effort to synthesize monodisperse oxide nanocrystals, here we report on the synthesis and characterization of uniform tetragonal zirconia nanocrystals via a nonhydrolytic sol−gel route. The nonhydrolytic sol−gel process has been extensively applied to synthesize various oxide nanostructured materials.[27,28] The Colvin group and other groups reported the nonhydrolytic sol−gel synthesis of titania nanoparticles. The resulting nanoparticles, however, had a broad particle size distribution or poor crystallinity.[12b,29,30]

The current synthesis relies upon a nonhydrolytic sol−gel reaction between zirconium(IV) isopropoxide and zirconium(IV) chloride at 340 °C. In this manner, we were able to synthesize multigram quantities of uniform-sized nanoparticles without a size selection process. The following describes the detailed synthetic procedure. First, 20 mmol (7.8 g) of zirconium(IV) isopropoxide propanol complex ($Zr[OCH(CH_3)_2]_4 \cdot (CH_3)_2CHOH$, Aldrich Chemical Co. 99.9%) and 25 mmol (5.83 g) of zirconium(IV) chloride (Aldrich Chemical Co. 99.9%) were added to 100 g of purified and degassed trioctylphosphine oxide (TOPO, Aldrich Chemical Co. 90%, purified by vacuum distillation) at 60 °C in an argon atmosphere. The temperature of the reaction mixture was raised slowly to 340 °C and held at this temperature for 2 h with vigorous stirring. During this thermal treatment, the initial light yellow solution color was changed to green. The reaction mixture was then cooled to 60 °C, and 500 mL of dried and degassed acetone was added to precipitate zirconia nanoparticles. The precipitate was retrieved by centrifugation and washed several times with acetone to remove excess TOPO, producing deep green colored zirconia nanoparticles. Under an optimized synthetic condition, we can synthesize over 5 g of product, which is an extremely large-scale production in the colloidal chemical synthesis of monodisperse nanoparticles. The zirconia nanoparticles produced can be readily redispersed in nonpolar organic solvents such as hexane and toluene.

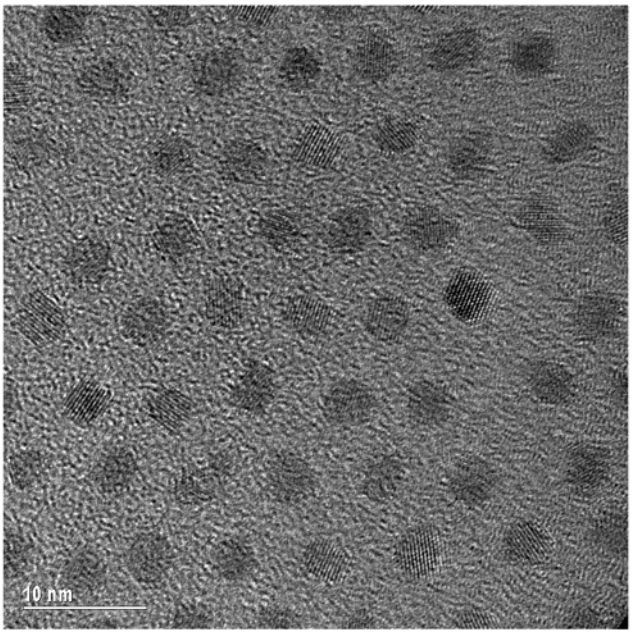

Figure 1. High-resolution TEM (HRTEM) image of 4.0 nm zirconia nanocrystals.

High-resolution transmission electron microscopic (HRTEM) images of the zirconia nanoparticles, as shown in Figure 1, show that the particles have a highly uniform particle size distribution with a particle size of 4.0 nm and that they are highly crystalline. Low-magnification TEM images also reveal the uniform particle size distribution of the nanoparticles (Supporting Information). These monodisperse and highly crystalline nanocrystals were synthesized directly without any size selection process, which is extremely important for large-scale production.

To investigate the mechanism of nanoparticle formation, we characterized the byproducts of the reaction by gas chromatography mass spectrometry (GCMS). The byproducts detected by GCMS were 2-chloropropane and propylene. The former seems to be produced from the nonhydrolytic sol−gel reaction between the zirconium alkoxide and the zirconium halide, that is, Zr-

(13) Badwal, S. P. S. *Appl. Phys. A* **1990**, *50*, 449.
(14) Garvie, R. C.; Hannink, R. H.; Pascoe, R. T. *Nature* **1975**, *258*, 703.
(15) Haw, J. F.; Zhang, J.; Shimizu, K.; Venkatraman, T. N.; Luigi, D.-P.; Song, W.; Barich, D. H.; Nicholas, J. B. *J. Am. Chem. Soc.* **2000**, *122*, 12561.
(16) Phillips, J. M. *J. Appl. Phys.* **1996**, *79*, 1829.
(17) León, C.; Lucía, M. L.; Santamaría, J. *Phys. Rev. B* **1997**, *55*, 882.
(18) Mansour, N.; Mansour, K.; Stryland, E. W. V.; Soileau, M. J. *J. Appl. Phys.* **1990**, *67*, 1475.
(19) (a) Wilk, G. D.; Wallace, R. M.; Anthony, J. M. *J. Appl. Phys.* **2001**, *89*, 5243. (b) Afanas'ev, V. V.; Houssa, M.; Stesmans, A.; Heyns, M. M. *Appl. Phys. Lett.* **2001**, *78*, 3073.
(20) Garvie, R. C. *J. Phys. Chem.* **1978**, *82*, 218.
(21) Moon, Y. T.; Park, H. K.; Kim, D. K.; Kim, C. H. *J. Am. Ceram. Soc.* **1995**, *78*, 2690.
(22) Stichert, W.; Schüth, F. *Chem. Mater.* **1998**, *10*, 2020.
(23) McCormick, P. G.; Tsuzuki, T.; Robinson, J. S.; Ding, J. *Adv. Mater.* **2001**, *13*, 1008.
(24) Xia, B.; Lenggoro, I. W.; Okuyama, K. *Adv. Mater.* **2001**, *13*, 1579.
(25) Rao, C. N. R.; Satishkumar, B. C.; Govindaraj, A. *Chem. Commun.* **1997**, 1581.
(26) Woudenberg, F. C. M.; Sager, W. F. C.; Sibelt, N. G. M.; Verweij, H. *Adv. Mater.* **2001**, *13*, 514.
(27) Vioux, A. *Chem. Mater.* **1997**, *9*, 2292.
(28) Tian, B.; Yang, H.; Liu, X.; Xie, S.; Yu, C.; Fan, J.; Tu, B.; Zhao, D. *Chem. Commun.* **2002**, 1824.
(29) Niederberger, M.; Bartl, M. H.; Stucky, G. D. *Chem. Mater.* **2002**, *14*, 4364.
(30) Parala, H.; Devi, A.; Bhakta, R.; Fischer, R. A. *J. Mater. Chem.* **2002**, *12*, 1625.

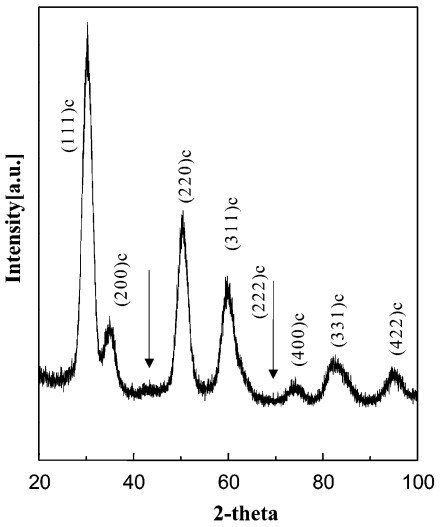

Figure 2. X-ray diffraction (XRD) pattern of zirconia nanocrystals.

Table 1. Summary of Reliability Factors of Rietveld Refinement for ZrO_2 Nanocrystals[a]

space group	R_p	R_{wp}	R_B	R_F	R_e	χ^2
$Fm\bar{3}m$	6.60	8.77	2.47	1.64	8.14	1.16
$P4_2/nmc$	6.49	8.60	2.29	1.62	8.14	1.14

[a] χ^2 (goodness of fit) $= (R_{wp}/R_e)^2$.

$$R_p = \frac{\sum |y_i(\text{obs}) - y_i(\text{calc})|}{\sum y_i(\text{obs})} \qquad R_{wp} = \left\{ \frac{\sum w_i (y_i(\text{obs}) - y_i(\text{calc}))^2}{\sum w_i (y_i(\text{obs}))^2} \right\}^{1/2}$$

$$R_e = \left\{ \frac{(N - P + C)}{\sum w_i y_i(\text{obs})} \right\}^{1/2} \qquad R_B = \frac{\sum |I_k(\text{obs}) - I_k(\text{calc})|}{\sum I_k(\text{obs})}$$

$$R_F = \frac{\sum |(I_k(obs))^{1/2} - (I_k(\text{calc})^{1/2})|}{\sum (I_k(\text{obs}))^{1/2}}$$

y_i(obs) and y_i(calc) are the observed and calculated intensities at the ith step, respectively, and I_k(obs) and I_k(calc) are the observed and calculated intensities asigned to the kth Bragg reflection. N is the total number of points, and P and C are the number of refined and constraint parameters. w_i is the weight factor.

$[OCH(CH_3)_2]_4 + ZrCl_4 \rightarrow 2ZrO_2 + 4(CH_3)_2CHCl$ (Supporting Information).[27] The latter seems to be generated by the dehydrochlorination of isopropyl chloride.

Figure 2 shows an XRD pattern of the ZrO_2 nanoparticles. All peaks can be assigned on the basis of a cubic structure, except the peaks indicated by an arrow in Figure 2. These extra peaks originate from a noncubic structure with lower symmetry. Because the tetragonal ($P4_2/nmc$) phase is slightly distorted from the cubic phase ($Fm\bar{3}m$) and peaks are broadened from the nanometer particle size, it is very difficult to differentiate between these two crystal phases using the X-ray diffraction pattern. Consequently, Rietveld refinement was carried out to determine the crystal structure of the ZrO_2 nanoparticles. Two model structures, cubic and tetragonal phases, were used to refine the crystal structure. As shown in Table 1, all reliability (R) factors refined from a tetragonal structure were lower than those refined from a cubic structure, although the R-factors of both structures were very similar. From these results, we conclude that the ZrO_2 nanocrystals are the tetragonal phase, and very close to a cubic phase. The refined parameters are summarized in the Supporting Information. As mentioned above, the formation of tetragonal undoped zirconia nanocrystals is important for many technological applications. The particle size calculated using the Sherrer formula was 3.1 nm. There are several reports on the fabrication of the high-temperature tetragonal zirconia phase, especially on thin film samples.[31] Garvie explained that tetragonal zirconia can be stabilized at room temperature without doping when the particle size is less than 10 nm.[20,32] The size effect is attributed to the lower surface free energy of the tetragonal form as compared to that of the monoclinic phase, which becomes more prominent for nanometer-sized particles. Differential thermal analysis and X-ray diffraction patterns obtained after heating at various temperatures of 400, 800, and 1200 °C showed that the tetragonal phase is stable up to 800 °C and then transformed to the monoclinic phase.

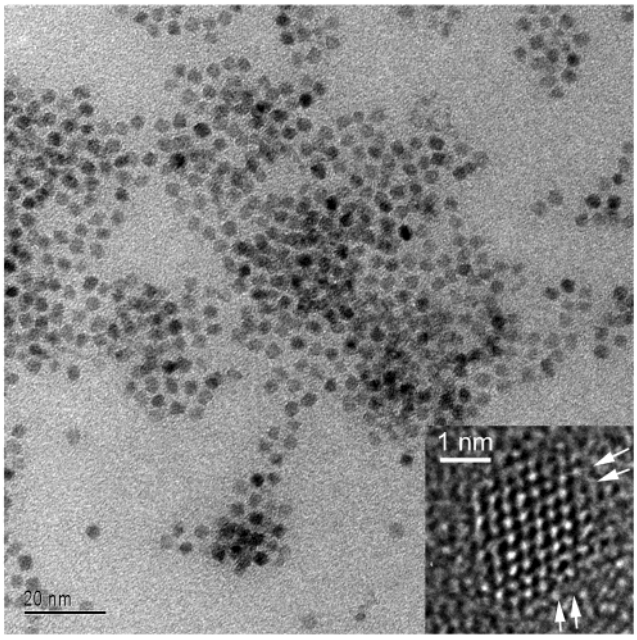

Figure 3. TEM image of 2.9 nm zirconia nanocrystals. The lattice image of a nanocrystal is shown in the inset with the lattice plane of {111} marked.

When zirconium(IV) bromide is used as a precursor instead of zirconium chloride while other experimental conditions were kept the same, zirconia nanoparticles with an average size of 2.9 nm were obtained. The TEM image of these nanoparticles (Figure 3) again exhibited a highly uniform particle size distribution, and a high-resolution TEM image of a single nanoparticle illustrated its highly crystalline nature with the {111} lattice plane shown.

The optical properties of 4 nm sized ZrO_2 nanoparticles have been characterized using electronic absorption and fluorescence spectroscopy. The electronic absorption and fluorescence spectra have been obtained using a Hewlett-Packard 8425A Diode Array UV−visible spectrometer and a Perkin-Elmer fluorometer (LS50B), respectively. Figure 4 shows a representative absorption spectrum and fluorescence spectrum of ZrO_2 nanoparticles. The absorption spectrum features weak absorption in the near UV and visible region that is most likely a result of transitions involving extrinsic states such as surface trap states or defect states.[33] The strong absorption starts at around 270 nm (4.6 eV),

(31) Codato, S.; Carta, G.; Rossetto, G.; Rizzi, G. A.; Zanella, P.; Scardi, P.; Leoni, M. *Chem. Vap. Deposition* **1999**, *5*, 159.
(32) (a) Garvie R. C. *J. Phys. Chem.* **1965**, *69*, 1238. (b) Garvie, R. C.; Goss, M. F. *J. Mater. Sci.* **1986**, *21*, 1253.

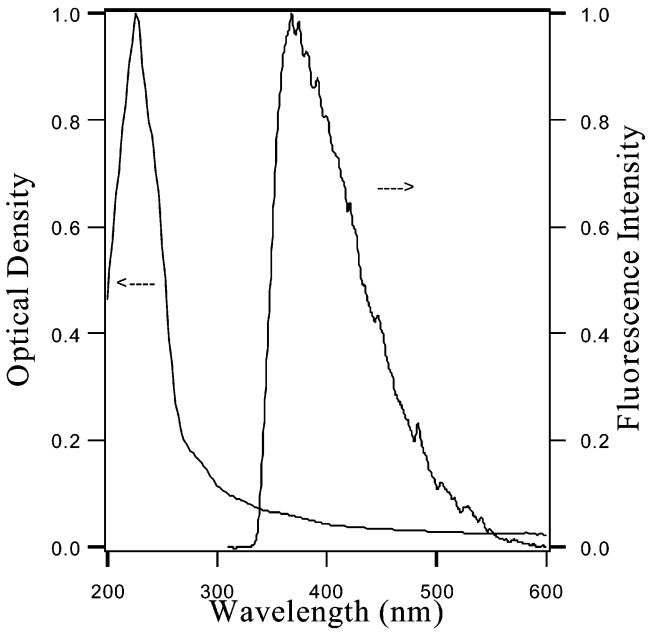

Figure 4. Representative electronic absorption spectrum (left) and static fluorescence spectrum (right) of ZrO_2 nanoparticles in cyclohexane. In the absorption spectrum, the optical density at 300 nm is 0.24. For the fluorescence spectrum, the sample was excited at 300 nm, and the spectrum was recorded with a 350 nm cutoff filter to block the scattered light of 300 nm. The filter most likely contributed toward the asymmetry of the fluorescence peak, and the true fluorescence yield should be higher than what is estimated based on the measured spectrum.

lower in energy as compared to the reported optical band gap of 5.0 eV for bulk ZrO_2.[33] This indicates that there is still contribution from extrinsic states toward absorption in this region.

Fluorescence spectra were measured with several excitation wavelengths from 260 to 390 nm. While the fluorescence intensity changes somewhat with excitation wavelength, the fluorescence peak position and band shape remained about the same for excitations below 350 nm. This indicates that the fluorescence involves the same initial and final states even as the excitation wavelength was varied between 260 and 350 nm, suggesting fast relaxation from the final state reached by photoexcitation to the states from which the fluorescence originates. Figure 4 shows one representative fluorescence spectrum with excitation at 300 nm. The spectrum features a broad fluorescence band centered around 370 nm with a fwhm of about 80 nm. The fluorescence band appears to be asymmetric because of the 350 nm cutoff filter used to block off scattered incident light at 300 nm. The broad nature of the band and the substantial red-shift of the peak position as compared to the bulk band gap strongly indicate that the fluorescence involves extrinsic states.[33] Because the particle size distribution is very narrow, the broad fluorescence band seems to be mostly caused by inhomogeneous broadening from a distribution of surface or defect states. The fluorescence quantum yield has been calculated by integrating the fluorescence band of ZrO_2 nanoparticles in cyclohexane and comparing it to that of perylene in ethanol. The calculated yields for excitation at 390, 300, and 260 nm are 0.30%, 0.39%, and 0.44%, respectively, assuming that the fluorescence quantum yield of perylene in ethanol excited at 390 nm is 99%.[34]

It has been shown previously that the fluorescence of ZrO_2 powder and colloidal particles is sensitive to molecules such as oxygen in the solvent.[33] We have studied the influence of oxygen on the fluorescence of ZrO_2 nanoparticles by bubbling Ar through ZrO_2 nanoparticles in hexane and comparing it to that without Ar bubbling. There appears to be little difference in the fluorescence spectra with and without bubbling with Ar. The independence of fluorescence on oxygen is different from previous studies where the presence of oxygen decreases the fluorescence in ZrO_2 nanoparticles.[33] It was suggested that the irradiation of oxygenated ZrO_2 sols yields trapped holes at surface defect centers, therefore increasing the rate of nonradiative recombination of free electrons with such centers. The fact that the fluorescence of ZrO_2 nanoparticles studied here is not affected by oxygen indicates that they are well capped by surfactants (TOPO) and have a relatively low density of surface states. This is consistent with the relatively strong luminescence observed, because most metal oxide nanoparticles show very weak or no detectable luminescence at room temperatures.[35] Therefore, the ZrO_2 nanoparticles synthesized in this study are of high quality in terms of both narrow size distribution and surface properties.

The high quality of the sample is most likely due to capping of the nanoparticles with TOPO. To access the interaction between TOPO and the nanoparticles, an FTIR spectrum of the ZrO_2 nanoparticles has been obtained by using a Perkin-Elmer 1600 series FTIR spectrometer (Supporting Information). The key difference between the spectra of the pure solvent (hexane) and the TOPO-capped ZrO_2 nanoparticles in hexane is the broad band at 1065.4 cm^{-1} that is present only for the nanoparticles. Typically, the P═O stretching mode in TOPO shows up at the position around 1190 cm^{-1}.[36,37] The 1065.4 cm^{-1} mode is tentatively attributed to the P═O stretching mode in TOPO molecules bound to the ZrO_2 nanoparticles through the O atom in P═O. The substantial red-shift of the P═O frequency is plausible because binding of TOPO to the ZrO_2 nanoparticle surface could significantly decrease the frequency of the P═O stretching mode.

In summary, highly crystalline and monodisperse tetragonal zirconia nanoparticles with a particle size of 4 nm were synthesized by the nonhydrolytic sol−gel reaction between zirconium(IV) isopropoxide and zirconium(IV) chloride at 340 °C. Smaller 3 nm sized zirconia nanoparticles were synthesized using zirconium(IV) bromide as a precursor instead of zirconium chloride. A fluorescence spectrum of 4 nm sized zirconia nanoparticles with excitation at 300 nm showed a broad fluorescence band centered around 370 nm. The optical studies also suggest that the nanoparticles are of high quality in terms of narrow particle size distribution and relatively low density of surface trap states. The synthetic method developed here is potentially useful for large-scale production of useful tetragonal zirconia nanocrystals.

Acknowledgment. T.H. would like to thank the National Creative Research Initiative Program of the Korean Ministry of Science and Technology for financial support. J.Z.Z. ac-

(33) Emeline, A.; Kataeva, G. V.; Litke, A. S.; Rudakova, A. V.; Ryabchuk, V. K.; Serpone, N. *Langmuir* **1998**, *14*, 5011.
(34) Melhuish, W. H. *J. Phys. Chem.* **1961**, *65*, 229.
(35) Cherepy, N. J.; Liston, D. B.; Lovejoy, J. A.; Deng, H.; Zhang, J. *J. Phys. Chem. B* **1998**, *102*, 770.
(36) Pouchert, C. J. *The Aldrich Library of FT-IR Spectra*, 1st ed.; Aldrich Chemical Co.: Milwaukee, WI, 1985.
(37) Lorenz, J. K.; Ellis, A. B. *J. Am. Chem. Soc.* **1998**, *120*, 10970.

knowledges support by the Petroleum Research Fund administered by the American Chemical Society. H.M.P. acknowledges the Korean Ministry of Science and Technology for the financial support through the NRL program. We would like to thank Prof. Han-Ill Yoo for the helpful discussion on zirconia structure characterization.

Supporting Information Available: Low-magnification TEM of 4 nm sized zirconia nanocrystals. GCMS of byproducts from reactions. Observed, calculated, and difference XRD profiles for ZrO_2 nanoparticles using Rietveld refinement. FTIR spectra of 4 nm sized ZrO_2 nanocrystals. Crystal data and structure refinement data of 4 nm sized ZrO_2 nanoparticles (PDF). This material is available free of charge via the Internet at http://pubs.acs.org.

JA034258B